**RESEARCH**

# Effect of surface retaining elements on rock stability: laboratory investigation with sand powder 3D printing

Hao Feng[1] · Lishuai Jiang[1] · Qingwei Wang[1] · Peng Tang[1] · Atsushi Sainoki[2,3] · Hani S. Mitri[4]

## Abstract

This study aims to investigate the beneficial effects of surface retaining elements (SREs) on the mechanical behaviors of bolted rock and roadway stability. 3D printing (3DP) technology is utilized to create rock analogue prismatic specimens for conducting this investigation. Uniaxial compression tests with acoustic emission (AE) and digital image correlation techniques have been conducted on 3DP specimens bolted with different SREs. The results demonstrate that the strength and modulus of elasticity of the bolted specimens show a positive correlation with the area of the SRE; the AE characteristics of the bolted specimens are higher than those of the unbolted specimen, but they decrease with an increase in SRE area, thus further improving the integrity of the bolted specimens. The reinforcement effect of SREs on the surrounding rock of roadways is further analyzed using numerical modelling and field test. The results provide a better understanding of the role of SREs in rock bolting and the optimization of rock bolting design. Furthermore, they verify the feasibility of 3DP for rock analogues in rock mechanics tests.

**Keywords** Roadway stability · Surface retaining element · Sand-powder · 3D printing · Rock bolting · Numerical modelling

## 1 Introduction

The stability of roadways in underground coal mines is a long-lasting concern due to its paramount importance in ensuring safe and efficient mining operations. Compared to other underground engineering (e.g., metal mining, tunneling, etc.), the ground control in coal mine roadways is more challenging due to the weak and fractured rock mass conditions, continuous geotechnical disturbances (longwall mining, strata collapse, fault-slip, etc.) and limited support costs (Peng 2008; Bobet and Einstein 2011).
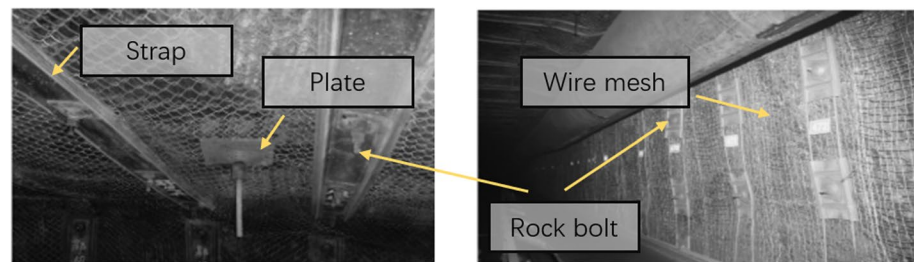
✉ Lishuai Jiang
   lsjiang@sdust.edu.cn

1  State Key Laboratory of Mining Disaster Prevention and Control, Shandong University of Science and Technology, Qingdao 266590, China

2  Faculty of Advanced Science and Technology, Kumamoto University, Kumamoto 860-8555, Japan

3  International Research Organization for Advanced Science and Technology, Kumamoto University, Kumamoto 860-8555, Japan

4  Department of Mining and Materials Engineering, McGill University, Montreal H3A 0E8, Canada

To date, rock bolting is the dominant supporting method for coal mine roadways (Thompson et al. 1999; Guo et al. 2013; Kang et al. 2010). Surface retaining elements (SREs) such as plates, straps, and wire meshes play an indispensable role in rock bolting systems. These elements are needed to form a support system by integrating all support elements and to transfer the load between the rock and support (Fig. 1) (Kang et al. 2010; Li 2017). The significance of SREs becomes even more pronounced when roadway stability is especially difficult to be maintained, such circumstances include but are not limited to weak and broken rock masses and high in situ stress. The SREs and their links to the bolts are considered the weak point of a rock support system, and the failure of one element can compromise the support system and lead to roof accidents (Cai 2013; Stacey 2011).

Over the past few decades, studies on the mechanical properties and supporting mechanisms of these elements have received considerable attention from researchers worldwide. Researchers first focused on the mechanical behaviors and support performance of individual elements, and laboratory tests and function analyses were carried out on wire meshes and plates to investigate their mechanical behaviors, such as strength and deformability (Ortlepp 1983; Morton et al. 2007; Player et al. 2008; Gray 2019). The overall

performance and interactions between the bolts and SREs were investigated afterward (Kang et al. 2015) conducted comprehensive research on the interactions among rebar, plates and washers by means of laboratory tests, numerical modeling and field tests, and their results highlighted the contact surface and deformation compatibility between the plates and washers. Cui et al. (2011) analyzed the effect of the end plate of fully grouted rock bolts on the global stability of a tunnel with a simplified numerical procedure. Dolinar (2004) investigated the load-bearing capacity and stiffness of the support material, area and pre-tightening force of plates to identify the affecting parameters. Charette and Bennett (2017) verified the importance of the plate-bolt compatibility through dynamic tests.

One of the major working mechanisms of rock bolting is the reinforcement of bolted rock masses, whose overall rock mass properties are significantly improved (Peng 2008; Brady and Brown 2006). Quantitative analyses of the rock mass reinforcement effect were carried out with different methodologies. Analytical attempts have been made to study the equivalent properties of bolted rock (Bobet and Einstein 2011; Srivastava and Singh 2015) and the response (displacement and stress distribution, etc.) of bolted openings (Zou et al. 2016). Laboratory tests have always been a powerful method since the beginning of rock mechanics, and tests on bolted rock have been conducted abundantly. Researchers have carried out uniaxial compression tests (Sakurai 2010), tension tests (Wu et al. 2018), shear tests (Ferrero 1995) and pull-out tests (Sawwaf and Nazir 2006) on bolted rocks or analogues, and the results have shown a significant increase in the rock mechanical properties in deformation modulus, strength in compression, tension, and shear, etc. The effects of various rock bolting parameters on the reinforcement performance have also been investigated in detail. By means of both experimental and numerical analysis, Grasselli (2005) discussed the different mechanical responses of bolted rocks with respect to the change in the diameter, angle and material of the bolt. Other considered bolt parameters include the length, density and grout properties (Kilic et al. 2002; Srivastava and Singh 2014). However, as an essential part of the rock bolting system, the effect of the SRE on the overall mechanical behaviors of a bolted rock mass has not been adequately addressed.

Therefore, in this study, the mechanical behaviors of rock specimens bolted with different SRE designs are investigated with uniaxial compression tests, and the fracture and deformation evolutions are monitored and analyzed with acoustic emission (AE) and digital image correlation (DIC) techniques. Sand-powder 3D printing is employed to create uniform and large rock analogues. The reinforcement effect of SREs on roadway surrounding rock is further analyzed with numerical modelling and field test. The results of the presented research provide a deeper understanding of the importance of SREs in rock bolting and contribute to rock bolting design. In addition, the methodology of sand-powder 3D printing provides insights regarding rock analogue preparation, which is a common issue in multiple fields of rock mechanics and engineering.

## 2 Rock analogue based on sand-powder 3D printing

### 2.1 Applications of 3D printing in rock mechanics

Natural rock has a high degree of heterogeneity, making it difficult to generate consistent results from multiple tests, even if they are taken from the same rock body. Additionally, rock specimens are usually destroyed in most mechanical tests, meaning that repeat tests or investigations of other properties cannot be performed (Gell et al. 2019; Wu et al. 2016). To overcome such problems, the application of rock analogue/artificial material started since the beginning of rock mechanical testing and has become a major topic (Ivars et al. 2011; Smith et al. 2014). In terms of research on rock bolt reinforcement, bolted analogues made by cement (Sakurai 2010), concrete (Ferrero 1995) and gypsum (Xu and Zhou 2019) are widely employed. Spang and Egger (1990) conducted shear tests on concrete specimens with fully grouted bolts; Yang et al. (2020) investigated the reinforcement effect of pre-tensioned bolts on jointed cement specimens.

However, a common limitation shared by using either natural rocks or analogues is the difficulty of producing internal and complex defects. Use of a wire saw, water jet or filling molds can only create external and simple geometry

defects (Fedrizzi et al. 2018). To overcome these problems, the development of 3D printing has led to recent attempts all over the world (Tian and Han 2017).

The 3D printing (3DP) technology, also known as additive manufacturing, is capable of creating multiple identical specimens so that tests can be repeated, and hence more reliable conclusions can be drawn (Gell et al. 2019). More importantly, 3DP can be used to replicate the internal structure of rock mass, which is not possible using any previous artificial specimen technique (Squelch 2018; Suzuki et al. 2017; Zhao et al. 2023; Zhou and Zhu 2017). It is well known that the most essential part of using rock analogue is the similarity validation of the mechanical behaviors compared to the natural rock. 3DP can create specimens with a wide variety of materials following the structures from 3D digital modeling. According to the printing process, 3DP can be divided into fused deposition molding (FDM), stereolithography appearance (SLA), or binder jetting technology (BJT). Different technologies have unique prototyping principles and corresponding suitable printing materials, and they also have different applications in the rock field (Song et al. 2018). With laboratory testing, researchers have found that rock analogues printed by FDM and polylactic acid have difficulty directly simulating natural rocks (Jiang and Zhao 2015). The brittleness of analogues made by SLA and photosensitive resin was stronger than that of other materials, which makes it suitable for simulating hard rock (Zhou and Zhu 2017). In recent years, analogues made by BJT and sand powder have been found to be quite close to natural sandstone, thus providing a more rock-like porous structure and deposition process (Perras and Volger 2019).

Recent studies have revealed that sand-powder 3D printed analogues show good similarity in mechanical behaviors to sandstone and other rocks that are common in underground coal mining, such as similar peak strength and elastic-brittle deformation characteristics (Niu et al. 2023; Tian et al. 2023; Volger et al. 2017). In addition, different sand types, printing parameters and material ratio can make sand powder 3D printing analogues realize laboratory reproduction of rocks with different lithologies (Gomez et al. 2019). By investigating the strength in compression, tension and crack propagation, sand-powder 3D printing has been considered a promising technique for creating rock analogue (Tian and Han 2017; Primkulov et al. 2017). Gomez et al. (2019) investigated the mechanical and hydraulic characterization of reservoir sandstone analogues by sand-powder 3D printing. By optimizing the sand-powder 3D printing parameters, Xu et al. (2021) obtained the analogues with properties such as strength that are closer to those of rocks. Therefore, this technique has been applied in the present study to create large specimens with prefabricated boreholes for bolts.

## 2.2 Specimen preparation

To install multiple bolts and connect the SRE, a large-scale specimen is favorable, which is also one of the features of 3D printing. The dimensions of the four groups of specimens used in this study were 100 mm × 100 mm × 200 mm (width × thickness × height). They were 3D printed using the BJT of the VX1000 3D system by Voxeljet (Perras and Volger 2019), as shown in Fig. 2. The overall printing process involved five core steps: (1) Establishing a three-dimensional model of the specimens through SolidWorks software; (2) Slicing and layering the model in the VX1000 3D system; (3) Mixing the GS19 sand powder of a specified grain size (120 μm) with acid (acidic activator); (4) Alternating deposition of activated GS19 sand powder and furan resin binding material, which was selectively deposited on the build platform; and (5) Thermal curing of specimens in a furnace at a constant temperature.



(a) VX1000 3D printer
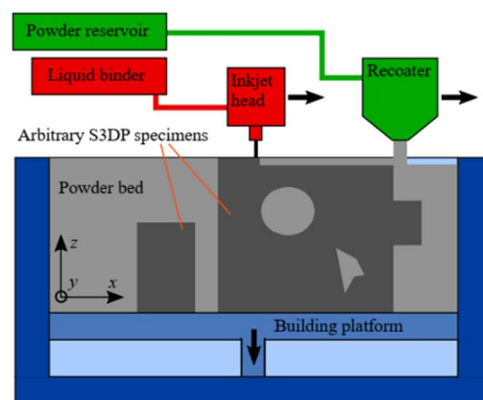


(b) Schematic elements of BJT (after Gomez et al. 2019)

**Fig. 2** The sand-powder 3DP system

While 3DP has been widely used for creating rock analogues, research on the mechanical properties of such analogues is still in its preliminary stage. The basis and premise for creating 3DP rock analogues with designed internal structure are, the similarity in mechanical behaviors between rock samples (intact from borehole drilling) and intact 3DP sample. Therefore, the specimens utilized in this study are intact specimen without any designed internal structure. Once the mechanical behaviors of sand powder 3DP rock analogues are confirmed, analogues with designed internal structures can be prepared based on CT scanning results. The unique advantages of preparing rock analogues with
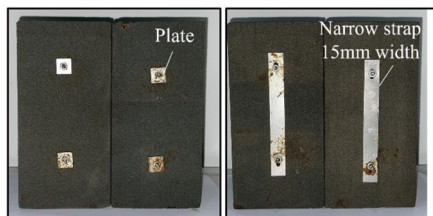
**Table 1** Test design

| Specimen ID | Classification | SRE | Dimensions of SRE $W$(mm)$\times L$ (mm) |
|---|---|---|---|
| US | Unbolted specimen | – | – |
| S1-1 | Scheme 1 | Plate | $15 \times 15$ |
| S1-2 | | | |
| S2-1 | Scheme 2 | Narrow strap | $15 \times 130$ |
| S2-2 | | | |
| S3-1 | Scheme 3 | Wide strap | $30 \times 130$ |
| S3-2 | | | |
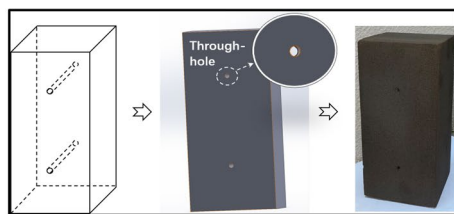
internal structures, boreholes for bolting can be prefabricated during the printing process (Fig. 3a).

To investigate the reinforcement effect of the SRE, proper simulation of the bolt and SRE in mechanical testing is essential. Selected based on previous studies (Yang et al. 2020), a steel bar (120 mm in length and 4 mm in diameter) is used to simulate the rock bolt, and a thin steel plate is used to simulate the SRE (Fig. 3b). As emphasized by Kang (2015) and Dolinar (2004), the area of the SRE is an important indicator to characterize the load transfer and surface protection capacity of the SRE. The area can not only characterize the structural properties of the SRE, but also indirectly characterize the mechanical properties by influencing the moment of inertia. It is a parameter that can comprehensively represent the overall performance of SRE. Therefore, four groups of specimens are designed and prepared, three groups of specimens are bolted with different SREs, and one group remains unbolted, as shown in Fig. 3c and Table 1. In each bolting specimen, two bolts are installed with grouting perpendicular to the loading direction, and the same amount of pre-tension force is applied to each specimen. Due to the microporosity of the sand-powder 3D printing analogue, a layer of Vaseline should be painted on the specimen surface before preparing the DIC speckle field to avoid the penetration of surface paint. After the Vaseline is dried, the black and white paint will be sprayed successively to form a speckle field (Fig. 3d). Due to the well homogeneous nature of 3DP, the properties of the specimens are consistent (Gell et al. 2019); therefore, only two specimens for each bolting group are prepared.

## 2.3 Test system and program

The RLJW-2000 rock servo-controlled testing system is applied to conduct the uniaxial compression test. The compression load is applied in the perpendicular direction in a displacement control mode, and its loading rate is 0.6 mm/min. The AE signal during the compression tests is
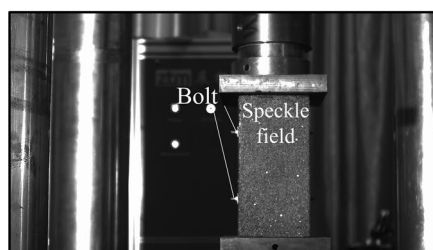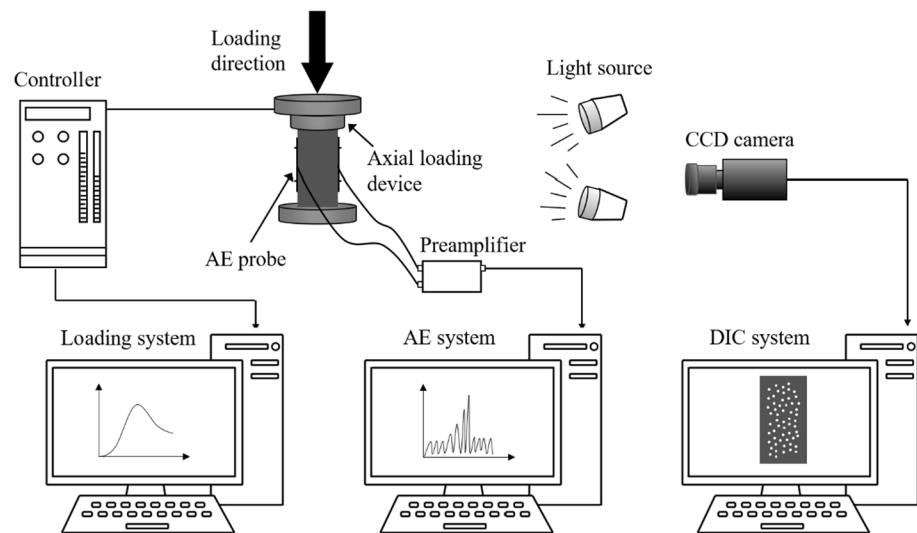


(a) 3D printed specimens with prefabricated boreholes



(b) Materials for bolting simulation



(c) Front view of bolted specimens



(d) Digital image correlation setup

**Fig. 3** Preparation of specimens

**Fig. 4** Uniaxial compression test system with AE and DIC monitoring



monitored with the Sensor Highway II system of PAC (Physical Acoustic Corporation), and its threshold is set to 45 dB. To better monitor the deformation of the specimen during the test, a high-speed camera is used to collect images of the speckle field at a rate of one sheet per second, and the collected speckle images are processed and analyzed by VIC-2D software. The related system and device are shown in Fig. 4.

## 3 Experimental study on the reinforcement effect of SREs

### 3.1 The influence of SREs on the mechanical behaviors of bolted rock

In Fig. 5a, the stress–strain curves of specimens under uniaxial compression are presented. The elastic–plastic mechanical characteristics of the sand-powder 3DP specimens and those of natural weak cemented sandstones are found to fall within a similar range (Bertuzzi 2002). This similarity is evident through the presence of the typical four stages, namely compaction, elastic, yielding, and post-peak stages, as well as brittle failure in each case. All the specimens showed notable compaction characteristics during initial loading, and then the stress gradually reached the peak value as the strain increased. In addition, the test data of sand-powder 3DP specimens in previous studies are similar to the results obtained in this study (Vogler 2017; Perras 2019).

The calculated mechanical properties of the specimens are listed in Fig. 5b and Table 2. It is evident that the rock bolting has a substantial effect in increasing the overall strength and rigidity of the bolted rock, thereby demonstrating the reinforcement effect. By installing the bolt and plate (comparing the results between US and S1), the strength

and modulus of elasticity of the specimens increased by 1.07 MPa and 0.09 GPa with increasing rates of 10.1% and 25.1%, respectively. It can be seen in the comparisons of S1, S2 and S3 that by replacing the plate with straps of different widths, the strength and modulus of elasticity further increased significantly. Bolted with narrow and wide straps, the strengths of the specimens reach up to 7.86 MPa and 7.82 MPa, and the modulus of elasticity increases to 1.36 GPa and 1.50 GPa. The increasing rate compared to Scheme 1 is 47.7% and 47.0% for strength and 40.1% and 54.3% for modulus of elasticity.

It can be concluded from the tests and analysis that the application of SREs in rock bolting can significantly increase the overall mechanical properties of bolted rock. The modulus of elasticity of the specimens shows a positive and dramatic correlation with the area of the SRE. As an important parameter defining the deformability of materials, the modulus of elasticity is directly related to the integrity of the rock mass according to the rock mass classification (Hoek et al. 2002). Therefore, the increase in the SRE area greatly contributes to the integrity of the bolted rock mass and thereby improves the deformation control and stability of the rock mass in field practice. In terms of rock strength, the change in results from S2 and S3 is negligible with the increase in SRE area, which indicates that the strength of the rock mass might not be linearly increased by simply increasing the area of the SRE. However, proper design of the SRE is still needed to ensure the rock mass strength.

### 3.2 The influence of SRE on the AE characteristics of bolted rock

The AE data generated during the loading process are associated with microcrack initiation, propagation, and
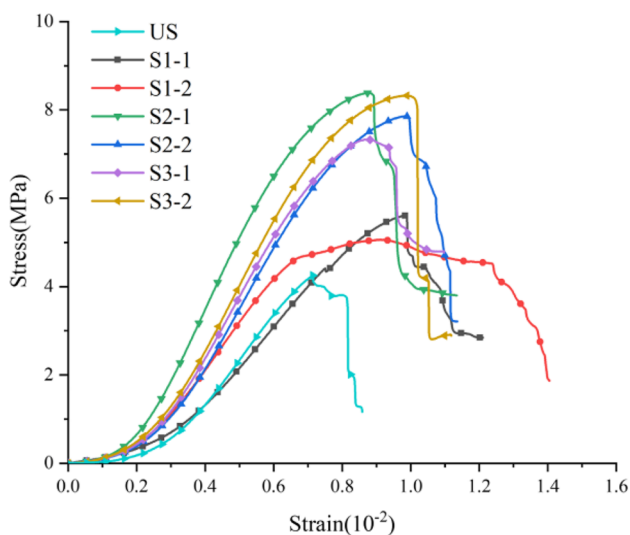
(a) axial stress–strain curves
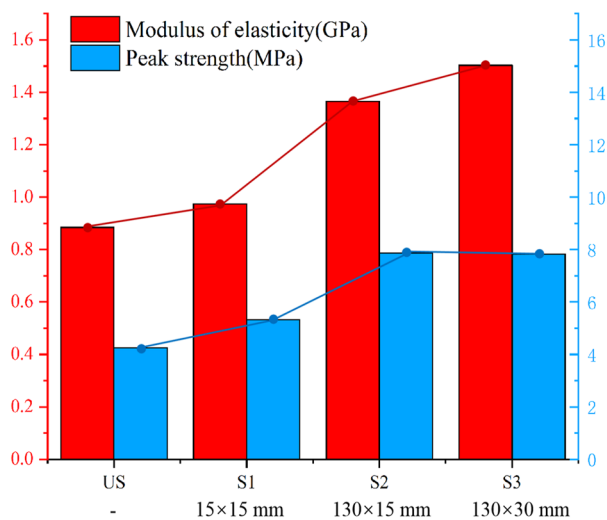


(b) strength parameters

**Fig. 5** Mechanical behaviors of specimens bolted with SREs

coalescence within the rock specimen. As mentioned in Sect. 3.1, while the mechanical behavior of each specimen is similar, there are still some specimens with discreteness

(scheme S1-2 has stronger ductility after the strength peak than others). To make the subsequent analysis of AE and DIC more representative, a group of schemes closest to their respective mean values should be selected according to the analysis results of elastic modulus and peak strength in the stress–strain curve, to characterize their overall characteristic. So, four specimens were picked out, US, S1-1, S2-2 and S3-2. In this section, the AE counts and AE energy are used to analyze the progressive fracturing characteristics of microcracks in the specimens. The stress–strain curves and the corresponding changes in the AE counts and AE energy against the loading time are shown in Figs. 6 and 7. The AE count and AE energy of the specimen under uniaxial compression exhibit a strong correlation with the stress–strain curve, displaying a similar changing trend. During the initial stage of loading, the internal microcracks within the specimens are gradually undergo compaction and closure. The AE counts and AE energy start to increase from the beginning of the compaction stage and then decrease after entering the elastic stage. As the load continues to increase, the specimens transition into the yielding stage, characterized by the development and expansion of new cracks. The interaction between cracks is intensified, and the expansion of cracks also shows a trend toward macroscopic crack aggregation. Both the AE counts and AE energy show a dramatic increase before the peak and continue as the crack continues to extend until the final failure.

The AE characteristics of the 4 groups of specimens show notable differences. The AE count and AE energy of the unbolted specimen remain at a relatively low level, while those of the bolted specimens are larger. For the unbolted specimen, the AE signal is not active before reaching the stress peak, and there is a long "quiet period". For the bolted specimens, high-frequency AE activities appear in the early stage of loading. Compared with unbolted specimens, the AE activities of bolted specimens is due to the slippage between bolt, binder and rock in addition to the closure of its own internal microcracks, which is consistent with the results obtained by other scholars (Tian et al. 2021). However, although the AE activities of the bolted specimens are greater than those of the unbolted specimen, the AE counts

**Table 2** Mechanical parameters of the specimen

| Specimen | Classification | Peak strength (MPa) | Average peak strength (MPa) | Modulus of elasticity (GPa) | Average modulus of elasticity (GPa) |
|---|---|---|---|---|---|
| US | Unbolted specimen | 4.25 | 4.25 | 0.88 | 0.88 |
| S1-1 | Scheme 1 | 5.60 | 5.32 | 0.91 | 0.97 |
| S1-2 | | 5.05 | | 1.03 | |
| S2-1 | Scheme 2 | 7.35 | 7.86 | 1.27 | 1.36 |
| S2-2 | | 8.38 | | 1.39 | |
| S3-1 | Scheme 3 | 7.33 | 7.82 | 1.46 | 1.50 |
| S3-2 | | 8.32 | | 1.61 | |

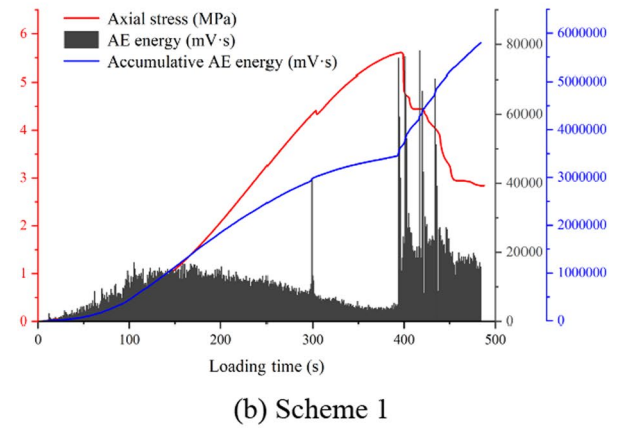(a) unbolted specimen

(b) Scheme 1

(c) Scheme 2

(d) Scheme 3
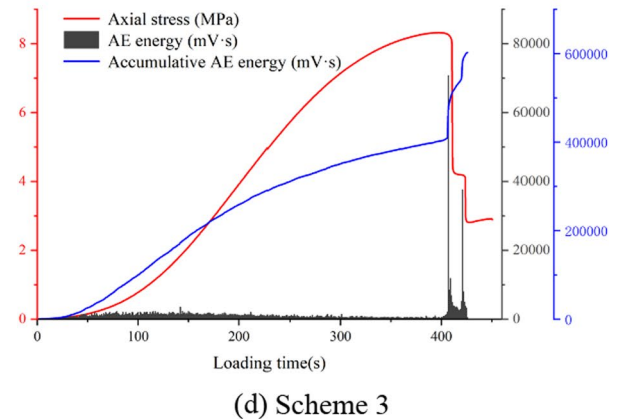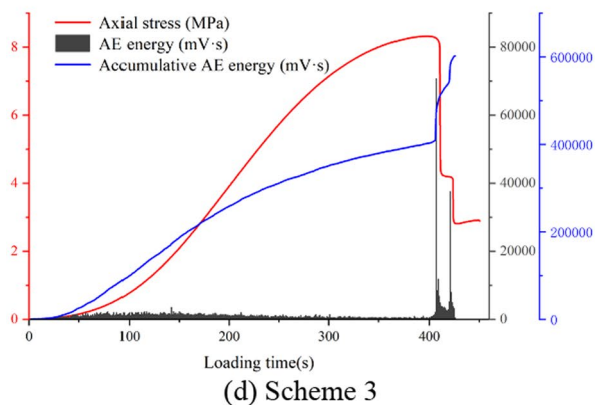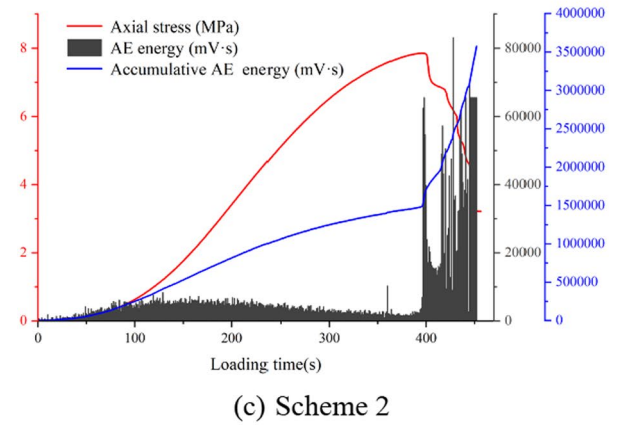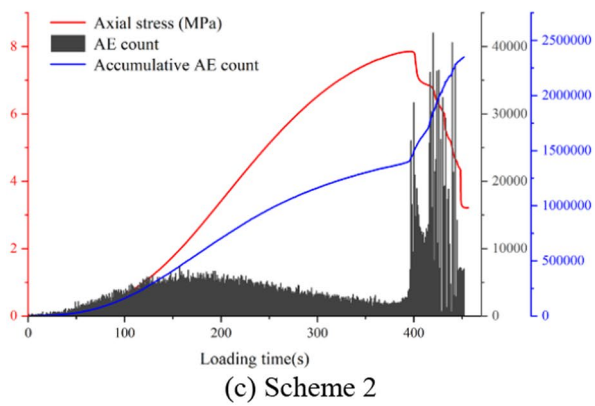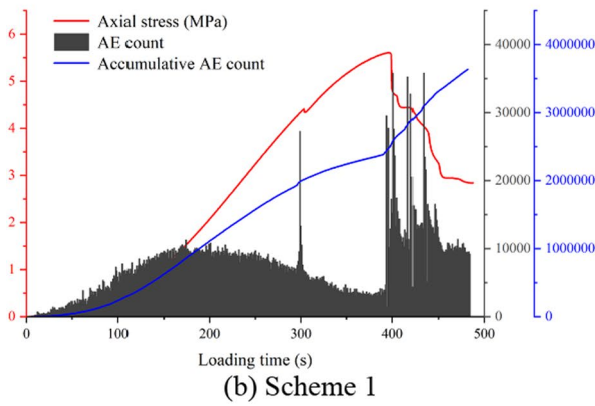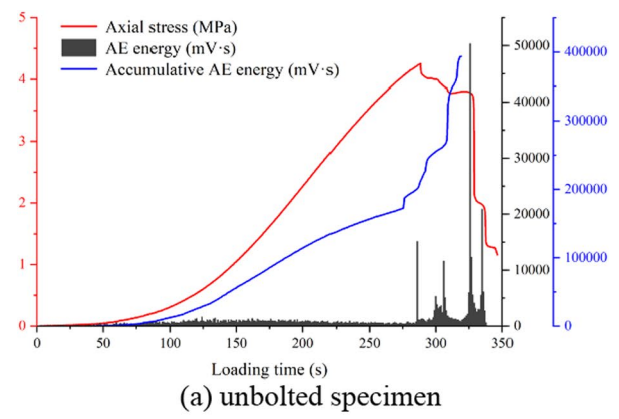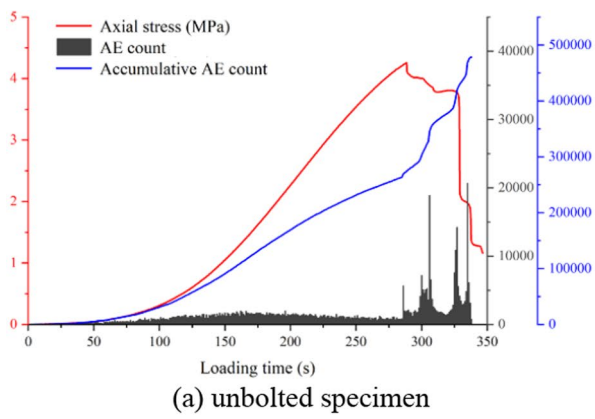
**Fig. 6** Evolution of the AE counts associated with the stress–strain relations for the specimens



(a) unbolted specimen

(b) Scheme 1

(c) Scheme 2

(d) Scheme 3

**Fig. 7** Evolution of the AE energy associated with the stress–strain relations for the specimens
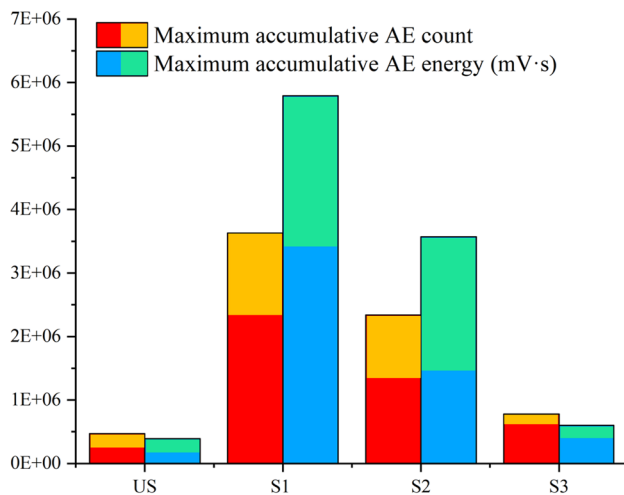
**Fig. 8** Relationship between AE characteristics and SRE

and AE energy will decrease with increasing SRE area. The AE count and energy are helpful to analyze the microcrack development characteristics at each stage during the loading process of the specimens, and their respective accumulation is helpful to the overall damage analysis of the specimen during the whole failure process. To conduct a more detailed analysis of the AE characteristics of the specimens, the maximum accumulative AE count and accumulative AE energy under different SREs are plotted in Fig. 8. The yellow color represents the accumulative count, while the cyan color represents the accumulative energy in the post-peak region. As can been seen, the SRE has a significant effect on reducing the AE activity and improving the stability of the bolted rock. Using of narrow straps (comparing the results between S1 and S2), the maximum accumulative AE count and accumulative AE energy of the specimens decreased by $1.29 \times 10^6$ and $2.22 \times 10^6$ mV s with decreasing rates of 35.3% and 38.3%, respectively. It can be seen in the comparison between S2 and S3 that by replacing the narrow straps with wide straps, the maximum accumulative AE count and accumulative AE energy further decreased by $1.56 \times 10^6$ and $2.97 \times 10^6$ mV s with decreasing rates of 66.6% and 83.1%, respectively. In addition, the accumulative AE count and energy of S3 in the post-peak region accounted for 21.7% and 33.1% of the total, respectively, which was the lowest among the four schemes. The use of wide straps will reduce the AE activity of specimens after peak, which means that the intensity of crack development and propagation at this stage will also be reduced.

The results show that the AE count and AE energy of bolted specimens are negatively correlated with SRE area; in particular, AE energy is more sensitive to SREs. Compared with the plate, the straps further constrain the deformation by connecting the bolts and forming a system, which leads to

a reduction in the slip and displacement of the bolts, thereby reducing the number of AE events. As an important parameter, AE energy reflects the intensity of the AE event and then can reflect the degree of damage to the rock. Therefore, the increase in the SRE area greatly contributes to the stable release of elastic strain energy of the bolted rock mass and thereby improves the stability of the rock mass.

### 3.3 The influence of SRE on the deformation and failure evolution characteristics of bolted rock

#### 3.3.1 Deformation evolution analysis

Digital image correlation (DIC) is a technical method used to measure the surface strain and deformation of an object by analyzing image-related points. It provides an intuitive and effective means of identifying the initiation, expansion, and evolution of fracture of the specimen. In this section, the Lagrange principal strain field under uniaxial compression is selected to quantitatively characterize the fracture evolution process of the specimen, as illustrated in Fig. 9. The stress state corresponding to each figure is also indicated. Due to the presence of the bolt and SREs, the strain field in Fig. 9 is monitored in the side view of the specimens shown in Fig. 3c.

For each test, as shown in Fig. 9, the principal strain distribution images of 4 characteristic points are selected to investigate the plane strain evolution. The 4 characteristic points are (1) The beginning of the yielding stage; (2) Middle of the yielding stage; (3) Peak point; and (4) Post-peak. It can be seen from the plane strain evolution that with continuous compression, notable strain concentrations gradually appear and develop until the final failure of the specimens. In the case of the unbolted specimen, the initiation point of crack is random and uncontrollable. However, for the bolted specimens, the bolts near the load end experience the first deformation under pressure during the uniaxial compression process (top to load). This deformation can impact the stability of the upper half of the specimens. At this time, the top of the specimens is in a weak state, and the maximum strain under the peak strain is often generated from this. Comparing the DIC images of Point (1) of different specimens, strain concentrations can be noticed in US and S1 when the stress reaches 80.5% (3.42 MPa) and 78.9% (4.42 MPa) of the peak. However, for S2 and S3, no notable strain concentrations are observed when the stress of the specimens reaches 78.0% (6.12 MPa) and 82.3% (6.85 MPa) of the peak. As the loading continues, the strain concentration of US and S1 further developed in both intensity and extent. When the stresses of S2 and S3 reach 92.3% (7.24 MPa) and 95.2% (7.92 MPa), respectively, of the peak, noticeable stress concentration zones occurred. Significant strain concentrations
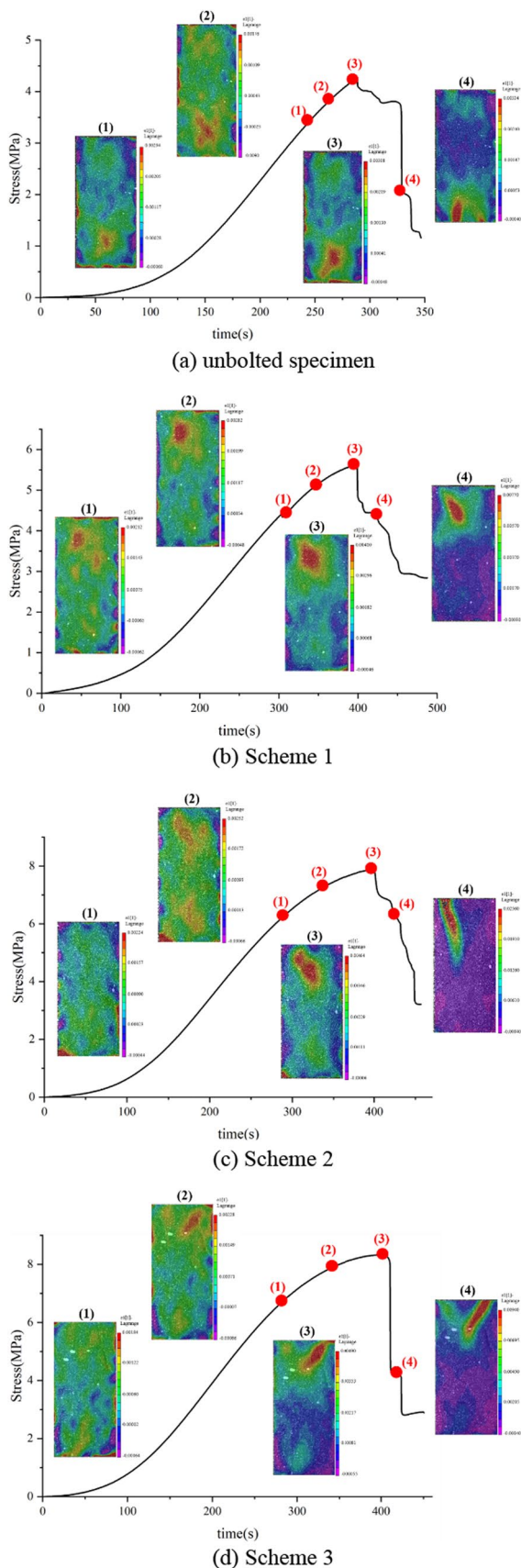
**Fig. 9** Evolution of the principal strain field

can be found in all four cases when the peak stress arrives, and the deformation persists until the final failure of specimens, which is also accompanied by the coalescence of primary and secondary cracks.

It can be shown by comparison that strain concentrations only occurred at a relatively higher stress level for specimens bolted with straps. In other words, under the condition of constant bolt spacing and length, the stress threshold for surface deformation and crack imitation has been raised due to the enhancement of SRE area. Such results indicate that the deformation-resistance capacity of rock can be significantly improved by increasing the surface protection of bolting, which can also be derived from the increase in the modulus of elasticity introduced in Sect. 3.1.

### 3.3.2 Failure pattern analysis

Figure 10 shows the final failure patterns of the specimens bolted with different SRE designs (S1, S2 and S3), and great differences can be noticed. It should be noted that both unbolted and bolt-plate-bolted (S1) specimens completely broke into several pieces after failure, and the S1 specimen was taped back into its original shape to investigate the failure and crack propagation pattern, as shown in Fig. 10a.

The failure pattern is significantly affected by the SRE. Three specimens bolted with SREs all experienced shear–tensile failure. For S1, the specimen completely broke, and dominate cracks occurred on both the bolted surface and unbolted surface. Additionally, one dominant crack emerged across the two bolting boreholes. By replacing the plate with a 15 mm strap, the S2 specimen did not completely break, which indicates an improvement in integrity. Two dominant cracks emerged on both surfaces, and the crack on the bolt surface occurred along the edge of the strap instead of between the boreholes. As the area of the SRE increases, the integrity of the S3 specimen further improves. A dominant crack only emerged on the unbolted surface, and no notable crack could be found in the bolted surface. By comparison, the increase in surface protection capacity provides extra
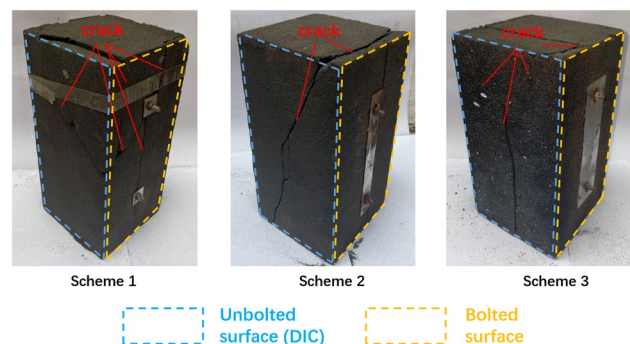


**Fig. 10** Failure pattern of the bolted specimen

restraint to the bolt surface and thereby improves the bolting effect and specimen integrity.

It should be noted that the failure patterns of specimens may be influenced by the printing process and parameters, i.e., the cohesion and distance between sand-powder particles.

# 4 Numerical analysis of the reinforcement effect of SRE

## 4.1 Model description

Although the reinforcement effect of SRE on the bolted rock was analyzed with experimental analysis, the underlying working mechanism remains to be further analyzed. For numerical simulation of roadway and other mine-wide scales, FLAC3D is a widely applied FDM method due to its high efficiency. In terms of the research content of this paper, the built-in structural element of FLAC3D is fully capable of simulating the mechanical behaviors of rock mass, support elements and their interactions, which is widely adopted by many scholars (Li 2018; Kang 2007). Figure 10 shows

the sectional view of a roadway FLAC3D model, which is built with a fine grid. In order to clearly reflect the stress field generated by the bolt, initial conditions are not applied to the model to analyze the influence of SRE on the stress distribution caused by the prestressed bolt. The bottom and perimeter of the model use fixed boundaries. The model boundaries are far enough away to eliminate their influence on the behavior of the modeled roadway. The entire domain of the model is coal with the following mechanical properties: density 1400 kg/m$^3$, Young's modulus 1.1 GPa, Poisson's ratio 0.32, internal friction angle 28°, cohesion 0.9 MPa, and tensile strength 0.12 MPa, which are estimated from the intact coal properties using the generalized Hoek–Brown failure criterion (Hoek 2002). The two support designs, namely, Design-A and Design-B, are simulated after the opening is created, and the only difference is the application of SREs, as shown in Fig. 11. The support simulation is achieved by utilizing the structural elements of the cable and beam in FLAC3D, and the relevant parameters of the elements are shown in Table 3. The stress distributions for the different supports are investigated after the model reaches equilibrium.



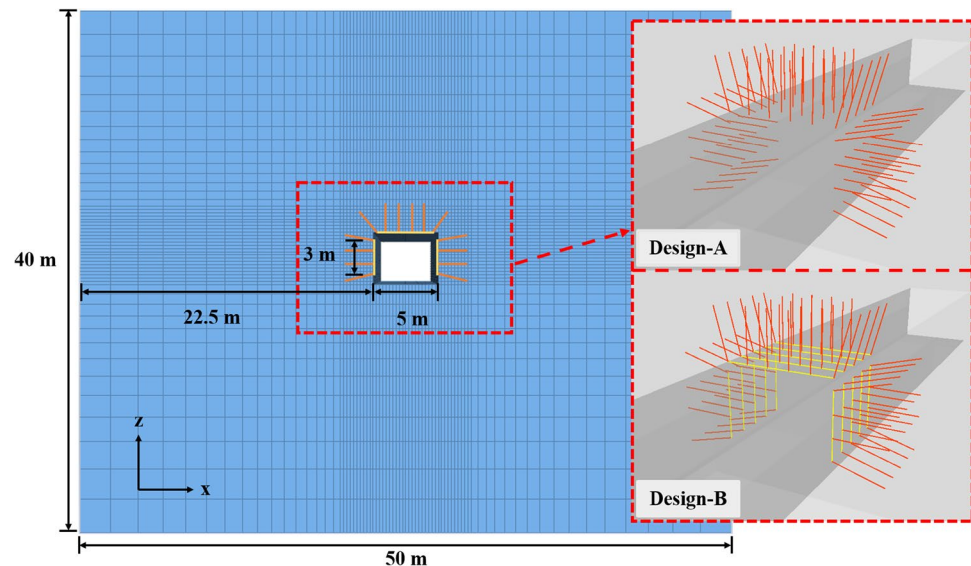**Fig. 11** FLAC3D roadway model and numerical simulation of support design

**Table 3** Parameters of supports in Design-A and B

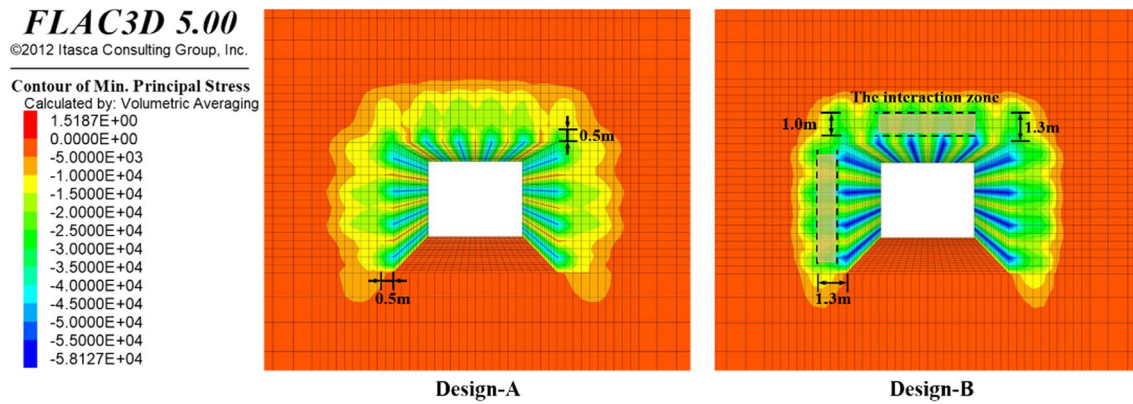| Item | Bolt length (mm) | Grout length (mm) | Diameter (mm) | Tensile strength (kN) | Pre-tension (kN) |
|---|---|---|---|---|---|
| Rebar bolt | 2400 | 1200 | 20 | 225 | 60 |
| | Width (mm) | Thickness (mm) | Poisson | Modulus of elasticity (GPa) | Moment of inertia (mm$^4$) |
| Steel strap | 280 | 3 | 0.3 | 210 | 540 |

**Fig. 12** Support stress distributions for with respect to the different support designs

**Fig. 13** Support stress distributions with respect to different support designs
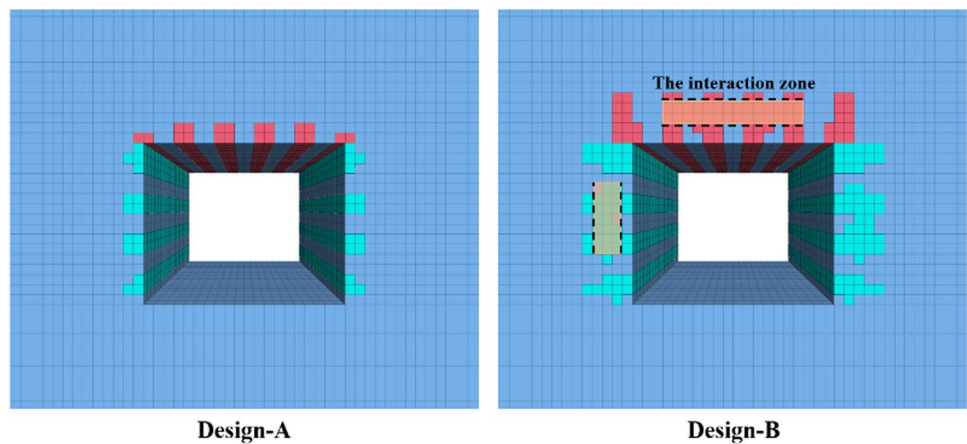


## 4.2 Simulation results

Since no additional stress field is applied to the roadway, the stress distribution within the roadway model is induced by rock support. In both cases, the same pre-tension of bolt was applied for both designs, and the area of stress in the roof and ribs was similar. However, the different degree of stress concentration may be one of the reasons for the difference in roadway stability in the real field. In Design-A (without SREs), the support stress is concentrated in the range of 0.5 m each on the ribs and the roof, and the stress concentration areas of each bolt are not connected to each other. In Design-B (with SREs), the support stress concentration of the ribs and the roof is further deepened, and the range is increased from 0.5 to 1.3 m. The stress concentration areas of the bolts are connected to each other to form an effective compressive stress zone, and the interaction zone can be clearly observed with a range of about 1.0 m.

In order to further study the stress distribution caused by the SRE, according to Fig. 12, the FISH code was used to identify the zone with principal stress greater than 20 kPa,

**Table 4** Distribution of the effective compressive stress zones with respect to different support designs

| Support design | Number of SZ in total | Number of SZ in the ribs (bule) | Number of SZ in the roof (orange) |
|---|---|---|---|
| Design-A | 1000 | 600 | 400 |
| Design-B | 3560 | 2000 | 1560 |

and divided it into effective compressive stress zone (SZ). The results are shown in Fig. 13 and Table 4. It can be easily observed that the distribution of SZs varies significantly among the support designs. Compared to Design-A, the SZs of Design-B is further extended, the SZs of the roof are 1560, and the SZs of the ribs are 2000, which are 2.3 times and 2.9 times of Design-A respectively. In addition, the interaction zone can also be observed.

According to the aforementioned analysis, Design-B generates a larger SZ area and a more uniform stress distribution than Design-A, while also having a more significant interaction zone. In the rock bolt support, the distributed

stress caused by the pre-tension of bolt is a critical parameter, and SRE is closely related to this distributed stress. Firstly, the use of SRE contributes to the distribution of the bolt pre-tension within the surrounding rocks. This results in a significant expansion of the effective compressive stress zone along the length of the SRE. As a result, an artificial pressure arch is formed, and the overlapping area of these zones, the interaction zone, further reduces the potential for deformation of surrounding rock between bolts. According to the pressure arch theory (Li 2017), the interaction zone ($t$) of bolt is an important factor affecting the supporting effect, which is determined by the reinforcement angle ($\alpha$), bolt spacing ($s$) and length ($L_b$), as illustrated in Fig. 14a. In this model, the reinforcement angle is generally considered to be 45°, and the effect of SRE is not taken into account, thus $t = L_b - a$. But the above numerical simulation results show that SRE significantly increases the range of the interaction zone, so a modified model is established, as shown in the Fig. 14b. In the modified model, we assume that the reinforcement angle $\alpha' = \alpha k$, where $k$ is related to the area, stiffness and structure of the SRE, and its empirical value ranges from 1.0 to 1.5. This value range is based on the enhancement amplitude of SRE on the mechanical properties of bolted body in the Sect. 3, and is comprehensively considered in combination with the research results of other scholars (Kang 2007). According to the geometric relationship, the interaction zone $t' = L_b - s/\tan \alpha'$. The thickness of the interaction zone ($t'$) and the reinforcement angle ($\alpha'$) increase due to the addition of additional SREs while keeping the identical bolt length ($L_b$) and spacing ($s$).

In addition, SRE spreads higher distributed stress from the rock surface to the depth of the rock, thereby improving the active support effect of the bolt. Noted that from the perspective of active support, SRE is an auxiliary element rather than a force-applying element, and its effect on stress spread is affected by the magnitude of the pre-tension force of the bolt. But it is undeniable that SRE is an important bridge for the mechanical transmission between the bolt and the surrounding rock, which determines whether the bolt can fully exert its intended function. Therefore, optimizing the design and implementation of bolts and SREs can effectively enhance ground stability.

# 5 Field application

It is of great significance to apply the laboratory test results to field practice for validation and further development of the obtained results. Therefore, a field practice study of roadway support design was conducted in Mataihao Mine, an underground coal mine in Inner Mongolia, China. Currently, the nearly horizontal seam being mined is 6.1 m in thickness at a depth of approximately 420 m. The case study was conducted in the tailentry of Panel 3105, an entry that was developed along the goaf of Panel 3103 with a 6-m-wide yield pillar, as shown in Fig. 15. Geological information (lithology, thickness, etc.) on the roof and floor strata was investigated by core logging. As the tailentry is driven in the middle of the coal seam, the immediate roof and floor is approximate 1-m-thick coal, and the main roof and floor of the target entry are composed of fine sand mudstone and sandy mudstone, respectively.

In order to characterize the strengthening of the overall physical properties of the bolted rock with strap rather
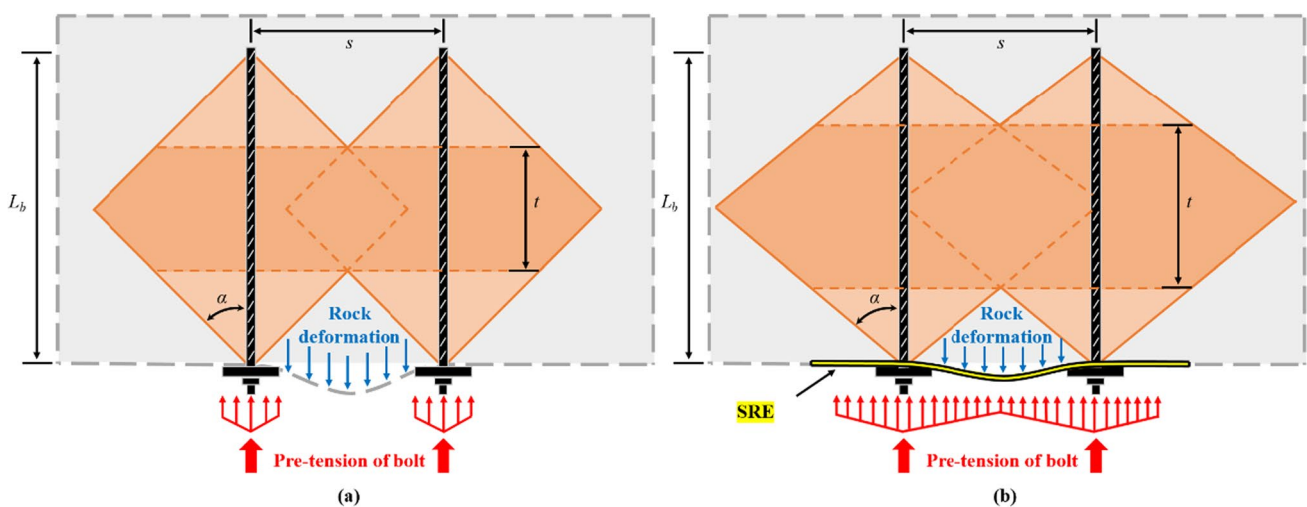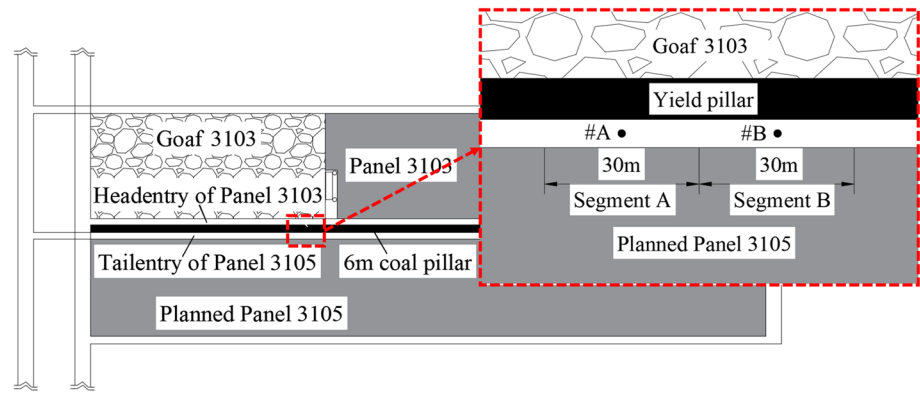


**Fig. 14** Reinforcement interaction between bolts with straps

**Fig. 15** Reinforcement interaction between bolts with straps



than the local displacement restriction, the segments were selected in locations where the surrounding rock are generally consistent to minimize the influence of geological heterogeneity. The measurement station was set between the straps. Two 30-m-long segments of the entry were selected to employ different support designs after excavation. Figures 16 and 17 shows the support designs of Segment A and B, the supporting system consists of pre-tensioned rebar and cable bolts and SREs. All rebar and cable bolts are partially grouted with resin cartridges, rebar bolts are used in both the roof and the ribs in a grid pattern of 1000 mm × 1000 mm, and cable bolts are installed in the roof with a spacing of 2000 mm between bolts and a spacing of 1000 mm between rows. For the support designs in Segment A and B, the application of rebar bolts, cable bolts and wire mesh are identical, the only difference is, cable traps with 4000 mm in length, 330 mm in width and 6 mm in thickness are installed on the roof, and cable traps with 3000 mm in length, 330 mm in width and 6 mm in thickness are installed on the two ribs. The purpose of designing such two support schemes is to practically investigate the effect on ground control with enhancing SREs.

Deformation monitoring was performed in each segment, and the collected data are shown in Fig. 17. As seen from the deformation data about 30 days of monitoring, the ground deformations vary with the support designs. At the end of the deformation monitoring program, the vertical roof-to-floor convergences of Segment A and B are 134. 4 mm and 95.0 mm, respectively, and the horizontal rib-to-rib convergences are 106.2 mm and 78.7 mm, respectively. By contrast, the support design in Segment B shows notable deformation-controlling effect in both vertical and horizontal direction with a decrease of 21.0% and 17.2%, which is contributed to the application of cable straps, which has been summarized as the reinforcement effect of SREs, as investigated with laboratory tests in Sect. 3 and analyzed in Sect. 4. It can be seen from the monitoring data, the behaviors and differences among the different

support designs have a certain degree of comparability. In the design of adding SRE, the deformation of the roof and rib decreased by 30–40 mm, which is in the same order of magnitude as that which can be reduced by other optimization designs considering bolt parameters. The above results provide a more reliable qualitative reference for the design of support system with SRE (Fig. 18).

# 6 Discussion

## 6.1 The methodology of sand-powder 3D printing

In this study, sand-powder 3DP is employed to create large-scale specimens. The test results from the same specimen group are relatively consistent due to the homogeneous nature of 3DP. Additionally, the mechanical behaviors, fracture propagations (AE and DIC data) and failure patterns of 3DP specimens are similar and representative of natural soft rocks; hence, the feasibility of using sand-powder 3DP in the field of rock mechanics is validated.

As known, one of the greatest challenges in the field of rock mechanics and engineering is the existence of discontinuities (faults, fractures, cracks etc.). Due to the presence of the discontinuities, the mechanical properties of the rock mass will greatly degrade, and the propagation and development of discontinuities will eventually lead to rock failure (Cao et al. 2016; Fan et al. 2021). The rock mechanics experimental research can be classified into two categories by means of the nature of the specimens: original rocks and rock-like analogs.

Commonly, jointed rock specimens would surely be more representative of the in-situ rock mass (Huang et al. 2020; Song et al. 2021), however, the shortcoming of this method lies on the difficulties in two aspects. Firstly, the current joint-creating techniques (waterjet, diamond saw etc.) have structural impact and damage on the rock specimens and generally only applicable to hard rock with high strength (Jiang and Zhao 2015). Secondly, the produced
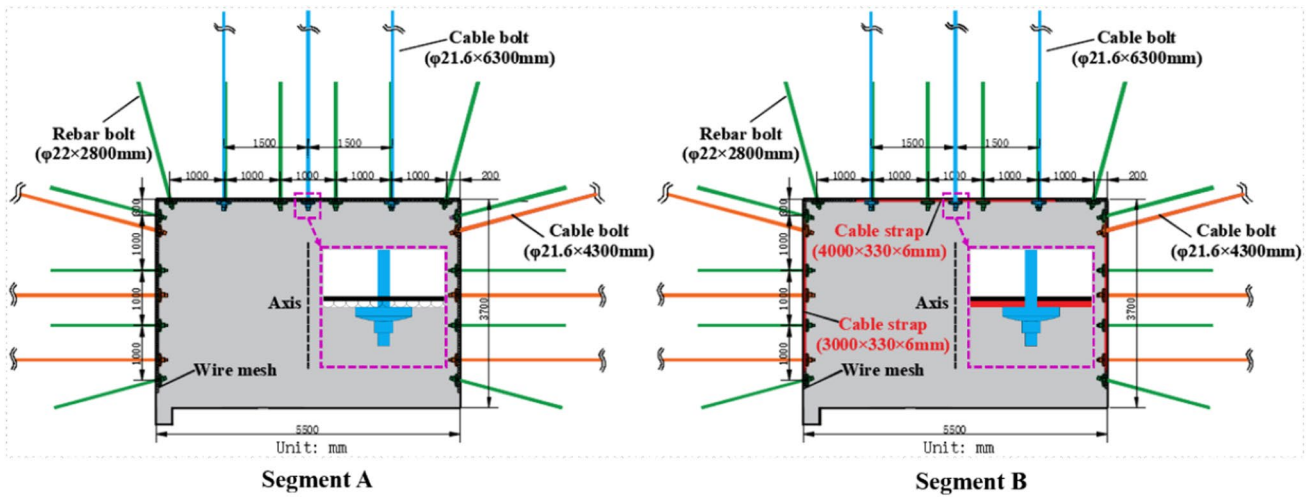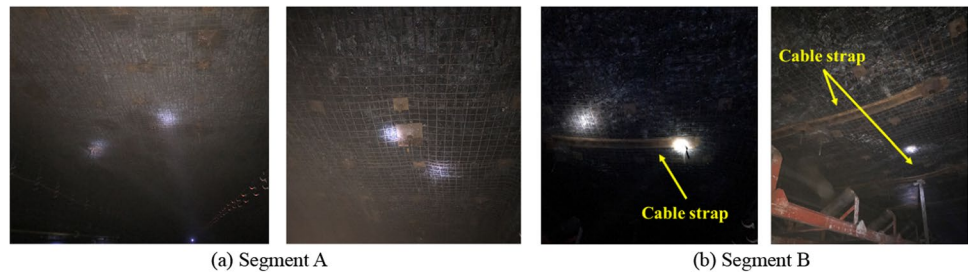
(a) Section view of entry
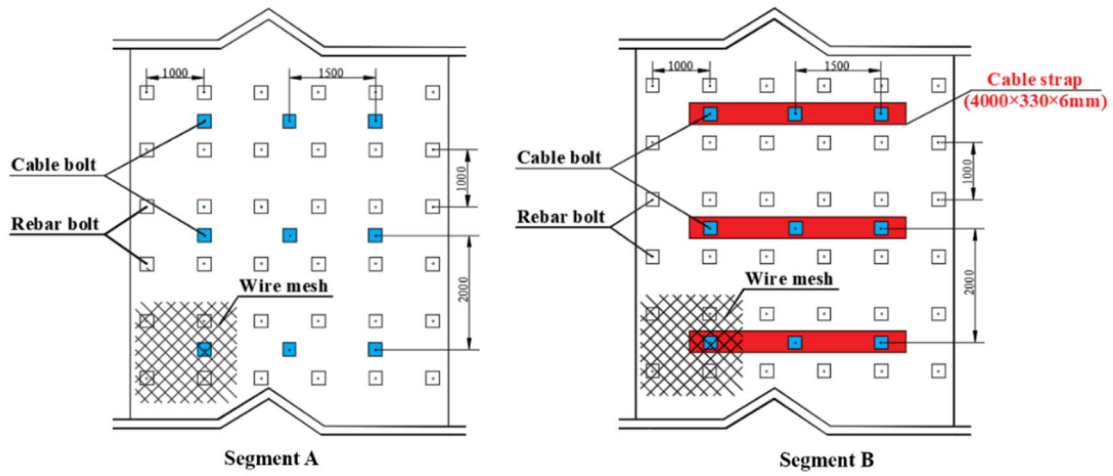


(b) Plan view of roof support
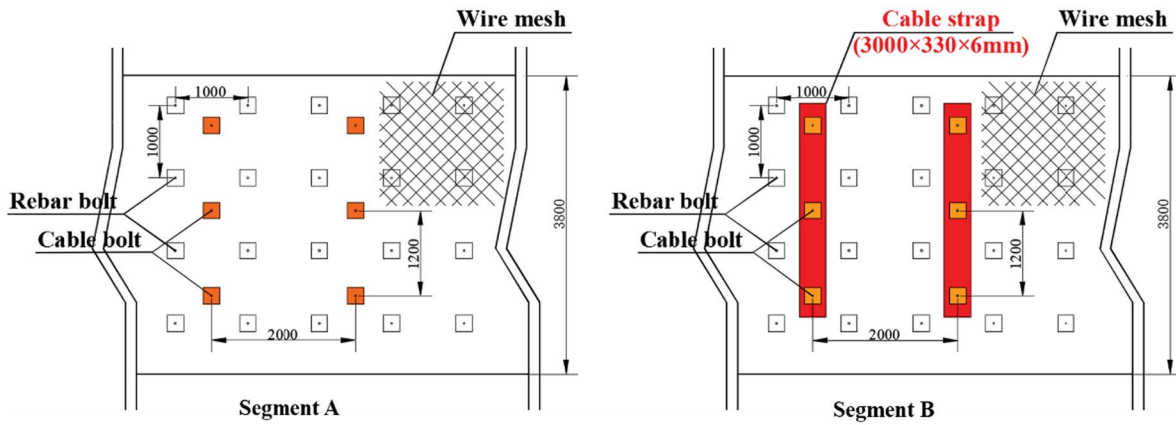


(c) Side view of rib support

**Fig. 16** Support designs of the two experimental segments

**Fig. 17** Support designs of the two experimental segments



(a) Segment A					(b) Segment B

joint structures (the number, shape and other geometric parameters) are limited with such techniques.

To investigate the mechanical behaviors of jointed soft rock, numerous attempts have been made with rock-like materials. It is well accepted that the rock-like specimens are helpful to reduce the effect of rock heterogeneity on the test results (Haeri et al. 2015; Fedrizzi et al. 2018). However, either natural rocks or analogues made by filling-molds methods share a common limitation, that is, the creation internal and complex-geometry defects in the specimens. It is obvious that using wire saw, water jet or filling moulds is only able to create external and simple-geometry defect.

The developing 3D Printing technology is capable of replicating the internal defect structure of rock masses (Ju et al. 2014; Suzuki et al. 2017), something which is not possible using any previous technique for making artificial rock specimens. And this technology can create multiple identical samples so that tests can be repeated and hence more reliable conclusions drawn (Squelch 2018; Sharafisafa et al. 2018; Gell et al. 2019), which making it an inspiring method for rock mechanics testing. Therefore,

it is essential to first validate the feasibility of using 3DP to simulate certain kind of specimen. In terms of this presented study, the application of the sand-power 3DP in creating rock-like bolted specimen is validated, which provide important basis for further research on the behaviors of jointed (even with fracture network) specimen and its bolting effect.

## 6.2 Reinforcement effect and application of SREs

In rock support practice, it's quite common to install extra rebar / cable bolts or use longer and strong bolts to improve the rock stability. However, this will definitely increase the economic and time cost of rock support, which needs to take the cost of drilling, labor and delay in entry development into account. The laboratory test, numerical simulation and field application results indicate that, the SREs are not only an auxiliary element, but rather an important part to effectively improve the stability of bolted rocks. Without increasing the number of bolts and other additional costs and labor conditions, adding SRE can still achieve a good supporting effect.
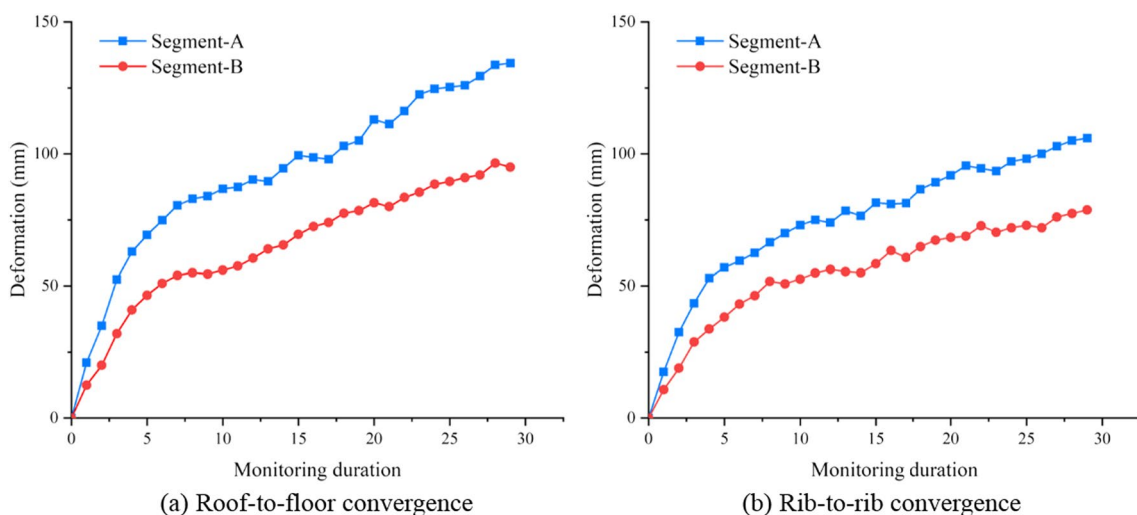


(a) Roof-to-floor convergence					(b) Rib-to-rib convergence

**Fig. 18** Deformation monitoring of the two segments

Due to the difficulty in conducting triaxial compressive test, shear test or Brazilian test on bolted specimens due to the testing mechanism (Zhu et al. 2018; Xu et al. 2019), the uniaxial compression strength is obtained to evaluating the strength-enhancing effect due to rock bolting. The results from Sects. 3 and 4 clearly suggest that the area of the SRE (i.e., the surface protection capacity) can effectively improve the mechanical responses and integrity of bolted rock. It is well accepted that proper support designs with pre-tensioned bolts and SREs can improve the stress state of rock masses and control their deformation and failure (Kang et al. 2017). By enlarging the area of SREs, the exposure of the rock surface and the rock falling potential are consequently decreased. More importantly, the load transfer between the rock and the support is enhanced, which includes the distribution of the bolt pre-tension force to the rock and the load and deformation of rock to the support elements.

The contribution of the presented results to ground control field practice is that the ground stability can be improved not only by simply increasing the parameters of the bolts (number, length, pretension, etc.) but also by conducting a comprehensive analysis to find the optimal and cost-efficient support design with the consideration of SREs. A good support design must be coordinated with all elements. The compatibility of these elements with each other determines the overall effectiveness and capacity of the overall ground support scheme (Thompson and Villaescusa 2014).

# 7 Conclusions

This study discusses the reinforcement effect of surface-retaining elements with sand-powder 3D-printed rock analogues. The mechanical behaviors, micro/macrocrack and deformation evolutions, and failure patterns of specimens under uniaxial compression are investigated with AE and DIC monitoring. The reinforcement effect of SREs on roadway surrounding rock is further analyzed with numerical modelling and field test. According to the experimental and numerical results, the following conclusions can be drawn:

(1) The application of SREs in rock bolting can significantly increase the overall mechanical properties of bolted rock, and the properties have a positive and dramatic correlation with the SRE area. When only the SRE area is changed, the strength of the bolted specimens with SRE was increased by 25.1%, 84.9%, and 84.0%, and the modulus of elasticity was increased by 10.2%, 54.5%, and 70.4%, respectively, compared with the unbolted specimen.

(2) The AE count and AE energy of the bolted specimen are significantly higher than those of the unbolted specimen, but they will decrease with increasing SRE area (close to the AE level of the unbolted specimen). A comparison of AE data indicates that the increase in SRE area greatly contributes to the stable release of elastic strain energy of the bolted rock mass and thereby improves the stability of the rock mass.

(3) By analyzing the DIC data, it is found that the stress threshold for surface deformation and crack imitation has been raised due to the enhancement of SRE area. Crack initiation only starts at a relatively higher stress level for specimens bolted with straps. As the SRE area increases, the integrity of the specimen further improves. A dominant crack only emerged on the unbolted surface, and no notable crack could be found in the bolted surface.

(4) The stress distribution caused by the bolt pre-tension is significantly improved after utilizing SRE, and the higher distributed stress spreads from the rock surface to the depth of the rock. The effective interaction zones are significantly enlarged, resulting in the enhancing of surrounding rock integrity and stability.

(5) By analyzing the monitoring data of the field practice, it is found that the deformation of the roof and ribs has been notably reduced by the application of cable strap, which has been summarized as the reinforcement effect of SREs. Behavior and differences between different support designs (with or without SRE) have a certain degree of comparability; hence, the test results have been validated and applied in field practice of rock support design.

With this comprehensive analysis of the mechanical, fracture, deformation and failure characteristics of bolted specimens, as well as the simulation and validation of the reinforcement effect of SRE in the roadway, the results of the presented research provide a deeper understanding of the importance of SREs in rock bolting and contribute to rock bolting design. In addition, these results also serve to validate the methodology of sand-powder 3D printing for soft rock analogues and provide insights for experimental research on rock mechanics.

## Declarations

**Competing interest** The authors declare that they have no known competing financial interests or personal relationships that could have appeared to influence the work reported in this paper.

## References

Bertuzzi R, Pells PJN (2002) Geotechnical parameters of Sydney Sand-stone and shale. Aust Geomech J 37(5):41–54. https://doi.org/10.3316/INFORMIT.812689394955021

Bobet A, Einstein HH (2011) Tunnel reinforcement with rockbolts. Tunnell Underground Space Technol Incorp Trenchless Technol Res 26(1):100–123

Brady B, Brown ET (2006) Rock mechanics for underground mining. Springer, Amsterdam

Cai M (2013) Principles of rock support in burst-prone ground. Tunnell Underground Space Technol Incorp Trenchless Technol Res 6:46–56

Cao R, Cao P, Lin H et al (2016) Mechanical behavior of brittle rock-like specimens with pre-existing fissures under uniaxial loading: experimental studies and particle mechanics approach. Rock Mech Rock Eng 49(3):763–783. https://doi.org/10.1007/s00603-015-0779-x

Charette F, Bennett A (2017) The importance of the face plate as part of an engineered holistic ground support scheme in dynamic conditions. In: Eighth international conference on deep and high stress mining. https://doi.org/10.1007/s00603-015-0779-x

Cui L, Sheng Q, Dong Y, Ruan B, Xu DD (2011) A quantitative analysis of the effect of end plate of fully-grouted bolts on the global stability of tunnel. Tunnell Underground Space Technol 114(2):104010

Dolinar DR (2004) Load capacity and stiffness characteristics of screen materials used for surface control in underground coal mines. Cem Concr Compos 26:389–404

Fan W, Yang H, Jiang X et al (2021) Experimental and numerical investigation on crack mechanism of folded flawed rock-like material under uniaxial compression. Eng Geol 291:106210

Fedrizzi RM, Ceia M, Misságia RM, Santos VH, Neto LI (2018) Artificial carbonate rocks: synthesis and petrophysical characterization. J Petrol Sci Eng 163:303–310

Ferrero AM (1995) The shear strength of reinforced rock joints. Int J Rock Mech Min Sci Geomech Abstr 32(6):595–605

Gray P (2019) Bearing plates: new developments in the unsung heroes of ground support. In: Aziz N, Kininmonth B (eds) Proceedings of the 1998 coal operators' conference. Mining Engineering, University of Wollongong, pp 18–20. https://ro.uow.edu.au/coal/257/

Gell EM, Walley SM, Braithwaite CH (2019) Review of the validity of the use of artificial specimens for characterizing the mechanical properties of rocks. Rock Mech Rock Eng 52(9):2949–2961. https://doi.org/10.1007/s00603-019-01787-8

Gomez JS, Chalaturnyk RJ, Zambrano-Narvaez G (2019) Experimental investigation of the mechanical behavior and permeability of 3d printed sandstone analogues under triaxial conditions. Transp Porous Media 129(2):541–557. https://doi.org/10.1007/s11242-018-1177-0

Grasselli G (2005) 3d behaviour of bolted rock joints: experimental and numerical study. Int J Rock Mech Min Sci 42(1):13–24

Guo X, Mao X, Ma C, Huang J (2013) Bolt support mechanism based on elastic theory. Int J Min Sci Technol 23:469–474

Haeri H, Khaloo A, Marji MF (2015) Experimental and numerical analysis of Brazilian discs with multiple parallel cracks. Arab J Geosci 8(8):5897–5908. https://doi.org/10.1007/s12517-014-1598-1

Hoek E, Carranza-Torres C, Corkum B (2002) Hoek-Brown failure criterion-2002 edition. Proc NARMS-Tac 1:267–273

Huang YH, Yang SQ, Bu YS (2020) Effect of thermal shock on the strength and fracture behavior of pre-flawed granite specimens under uniaxial compression. Theor Appl Fract Mech 106:102474

Ivars DM, Pierce ME, Darcel C, Reyes-Montes J, Potyondy DO, Young RP, Cundall PA (2011) The synthetic rock mass approach for jointed rock mass modelling. Int J Rock Mech Min Sci 48:219–244

Jiang C, Zhao GF (2015) A preliminary study of 3d printing on rock mechanics. Rock Mech Rock Eng 48(3):1041–1050. https://doi.org/10.1007/s00603-014-0612-y

Ju Y, Xie H, Zheng Z et al (2014) Visualization of the complex structure and stress field inside rock by means of 3D printing technology. Chin Sci Bull 59(36):5354–5365. https://doi.org/10.1007/s11434-014-0579-9

Kang HP, Jiang TM, Gao FQ (2007) Effect of pretensioned stress to rock bolting. J China Coal Soc 32(7):680–685

Kang HP, Wu YZ, Li JB (2010) Analysis on mechanical performances and supporting function of combination support elements for rock bolting. J China Coal Soc 35(7):9

Kang HP, Yang JH, Meng X (2015) Tests and analysis of mechanical behaviours of rock bolt components for China's coal mine roadways. J Rock Mech Geotech Eng 1:13

Kang HP, Li JZ, Yang JH, Gao FQ (2017) Investigation on the influence of abutment pressure on the stability of rock bolt reinforced roof strata through physical and numerical modeling. Rock Mech Rock Eng 50(2):387–401. https://doi.org/10.1007/s00603-016-1114-x

Kilic A, Yasar E, Celik AG (2002) Effect of grout properties on the pull-out load capacity of fully grouted rock bolt. Tunnell Underground Space Technol Incorp Trenchless Technol Res 17(4):355–362

Li CC (2017) Principles of rockbolting design. J Rock Mech Geotech Eng 9(3):19

Li WT, Yang N, Yang B et al (2018) An improved numerical simulation approach for arch-bolt supported tunnels with large deformation. Tunnell Underground Space Technol 77:1–12

Morton E, Thompson AG, Villaescusa E, Roth A (2007) Testing and analysis of steel wire mesh for mining application of rock surface support. ISRM Congress. https://onepetro.org/isrmcongress/proceedings-abstract/CONGRESS07/All-CONGRESS07/63133

Niu QJ, Jiang LS, Li CA (2023) Application and prospects of 3d printing in physical experiments of rock mass mechanics and engineering: materials, methodologies and models. Int J Coal Sci Technol 10(1):5. https://doi.org/10.1007/s40789-023-00567-8

Ortlepp WD (1983) Considerations in the design of support for deep hard-rock tunnels. Isrm Congress. https://onepetro.org/isrmcongress/proceedings-abstract/CONGRESS83/All-CONGRESS83/ISRM-5CONGRESS-1983-132/166696

Peng SS (2008) Coal mine ground control, 3rd edn. Peng SS Publisher, Morgantown, pp 229–237

Perras MA, Vogler D (2019) Compressive and tensile behavior of 3d-printed and natural sandstones. Transp Porous Media 129(2):559–581. https://doi.org/10.1007/s11242-018-1153-8

Player J, Morton E, Thompson A, Villaescusa E (2008) Static and dynamic testing of steel wire mesh for mining applications of rock surface support. In: International symposium on ground support in mining and civil engineering construction. https://www.saimm.co.za/Conferences/GroundSupport2008/693-706_Morton.pdf

Primkulov B, Chalaturnyk J, Chalaturnyk R, Zambrano-Narvaez G (2017) 3d printed sandstone strength: curing of furfuryl alcohol

resin-based sandstones. 3D Print Addit Manuf 4(3):149–155. https://doi.org/10.1089/3dp.2017.0032

Sakurai S (2010) Modeling strategy for jointed rock masses reinforced by rock bolts in tunneling practice. Acta Geotech 5(2):121–126. https://doi.org/10.1007/s11440-010-0117-0

Sawwaf ME, Nazir A (2006) The effect of soil reinforcement on pullout resistance of an existing vertical anchor plate in sand. Comput Geotech 33(3):167–176

Sharafisafa M, Shen L, Xu Q (2018) Characterisation of mechanical behaviour of 3D printed rock-like material with digital image correlation. Int J Rock Mech Min Sci 112:122–138

Smith SE, MacLaughlin MM, Adams SL, Wartman J, Applegate K, Gibson M, Arnold L, Keefer D (2014) Interface properties of synthetic rock specimens: experimental and numerical investigation. Geotech Test J 37:5

Song L, Jiang Q, Shi YE, Feng XT, Li Y, Su F, Liu C (2018) Feasibility investigation of 3d printing technology for geotechnical physical models: study of tunnels. Rock Mech Rock Eng 51(8):2617–2637. https://doi.org/10.1007/s00603-018-1504-3

Song Y, Tan H, Yang H et al (2021) Fracture evolution and failure characteristics of sandstone under freeze-thaw cycling by computed tomography. Eng Geol 294:106370

Spang K, Egger P (1990) Action of fully-grouted bolts in jointed rock and factors of influence. Rock Mech Rock Eng 23(3):201–229. https://doi.org/10.1007/BF01022954

Squelch A (2018) 3d printing rocks for geo-educational, technical, and hobbyist pursuits. Geosphere 14:1

Srivastava LP, Singh M (2014) Effect of fully grouted passive bolts on joint shear strength parameters in a blocky mass. Rock Mech Rock Eng 48(3):1–10. https://doi.org/10.1007/s00603-014-0615-8

Srivastava LP, Singh M (2015) Empirical estimation of strength of jointed rocks traversed by rock bolts based on experimental observation. Eng Geol 197:103–111

Stacey TR (2011) A philosophical view on the testing of rock support for rockburst conditions. J S Afr Inst Min Metall 112(8):01–08

Suzuki A, Watanabe N, Li KW, Horne RN (2017) Fracture network created by 3D printer and its validation using CT images. Water Resour Res 53:6330–6339. https://doi.org/10.1002/2017WR021032

Tan JN, Wang B, Feng T, Ning Y, Liu BB, Zhao FJ (2021) Acoustic emission characteristics of anchored sandstone under uniaxial compression and its correlation with rockburst. J Cent South (sci Technol) 52(8):2828–2838

Thompson AG, Villaescusa E, Windsor CR (1999) Rock support and reinforcement practice in mining. In: Proceedings of the international symosium on rock support kalgoorlie. https://sc.panda321.com/extdomains/books.google.com/books?hl=zh-CN&lr=&id=INy84pE47BUC&oi=fnd&pg=PA37&dq=Rock+support+and+reinforcement+practice+in+mining&ots=p-TBAjs6Xe&sig=c1mVeb5g3DoqdRTeGhjQHeck3Es

Thompson AG, Villaescusa E (2014) Case studies of rock reinforcement components and systems testing. Rock Mech Rock Eng 47(5):1589–1602. https://doi.org/10.1007/s00603-014-0583-z

Tian W, Han NV (2017) Mechanical properties of rock specimens containing pre-existing flaws with 3d printed materials. Strain 53:6. https://doi.org/10.1111/str.12240

Tian W, Wang XH, Yun W et al (2023) Mechanical properties of sand 3D printed rock-like samples based on different post-processing methods. Rock Soil Mech 44(05):1330–1352. https://doi.org/10.16285/j.rsm.2022.0886

Vogler D, Walsh S, Dombrovski E, Perras MA (2017) A comparison of tensile failure in 3d-printed and natural sandstone. Eng Geol 226:221–235

Wu B, Yao W, Xia K (2016) An experimental study of dynamic tensile failure of rocks subjected to hydrostatic confinement. Rock Mech Rock Eng 49(10):1–10. https://doi.org/10.1007/s00603-016-0946-8

Wu C, Chen X, Hong Y, Xu R, Yu D (2018) Experimental investigation of the tensile behavior of rock with fully grouted bolts by the direct tensile test. Rock Mech Rock Eng 51(1):351–357. https://doi.org/10.1007/s00603-017-1307-y

Xu RC, Zhou H (2019) Experimental investigation of the anchoring effect of two different types of rock bolts on fractured rock. Adv Mater Sci Eng 3:1–10

Xu Q, Jiang L, Ma C, Niu Q, Wang X (2021) Effect of layer thickness on the physical and mechanical properties of sand powder 3D printing specimens. Front Earth Sci. https://doi.org/10.3389/feart.2021.763202/full

Yang WD, Luo GY, Bo CJ, Wang L, Lu XX, Wang YN, Wang XP (2020) Mechanical properties and reinforcement effect of jointed rock mass with pre-stressed bolt. J Cent South Univ 27(12):3513–3530. https://doi.org/10.1007/s11771-020-4469-9

Zhou T, Zhu JB (2017) Identification of a suitable 3d printing material for mimicking brittle and hard rocks and its brittleness enhancements. Rock Mech Rock Eng 51(3):765–777. https://doi.org/10.1007/s00603-017-1335-7

Zhu WX, Jing HW, Yang LJ et al (2018) Strength and deformation behaviors of bedded rock mass under bolt reinforcement. Int J Min Sci Technol 28(4):7

Zou JF, Xia ZQ, Dan HC (2016) Theoretical solutions for displacement and stress of a circular opening reinforced by grouted rock bolt. Geomech Eng 11(3):439–455

Zhao Y, Jiang LS, Li, CA et al (2023) Experimental investigation into the mechanical behavior of jointed soft rock using sand powder 3D printing. Rock Mech Rock Eng 56:5383–5404. https://doi.org/10.1007/s00603-023-03346-8